



Contents lists available at ScienceDirect

Environmental Pollution

journal homepage: www.elsevier.com/locate/envpol

Air quality impacted by local pollution sources and beyond – Using a prominent petro-industrial complex as a study case[☆]



Sheng-Po Chen^{a, *}, Chieh-Heng Wang^b, Wen-Dian Lin^c, Yu-Huei Tong^c, Yu-Chun Chen^c, Ching-Jui Chiu^c, Hung-Chi Chiang^c, Chen-Lun Fan^c, Jia-Lin Wang^{d, **}, Julius S. Chang^a

^a Atmospheric Sciences Research Center, University at Albany, State University of New York, Albany, NY, USA

^b Center for Environmental Studies, National Central University, Taoyuan, Taiwan

^c Environmental Simulation CO. LTD., Taipei, Taiwan

^d Department of Chemistry, National Central University, Taoyuan, Taiwan

ARTICLE INFO

Article history:

Received 17 October 2017

Received in revised form

26 January 2018

Accepted 27 January 2018

Keywords:

Sulfur dioxide

Coastal air quality

Monitoring network

Model simulation

ABSTRACT

The present study combines high-resolution measurements at various distances from a world-class gigantic petrochemical complex with model simulations to test a method to assess industrial emissions and their effect on local air quality.

Due to the complexity in wind conditions which were highly seasonal, the dominant wind flow patterns in the coastal region of interest were classified into three types, namely northeast monsoonal (NEM) flows, southwest monsoonal (SEM) flows and local circulation (LC) based on six years of monitoring data. Sulfur dioxide (SO₂) was chosen as an indicative pollutant for prominent industrial emissions. A high-density monitoring network of 12 air-quality stations distributed within a 20-km radius surrounding the petrochemical complex provided hourly measurements of SO₂ and wind parameters. The SO₂ emissions from major industrial sources registered by the monitoring network were then used to validate model simulations and to illustrate the transport of the SO₂ plumes under the three typical wind patterns. It was found that the coupling of observations and modeling was able to successfully explain the transport of the industrial plumes. Although the petrochemical complex was seemingly the only major source to affect local air quality, multiple prominent sources from afar also played a significant role in local air quality. As a result, we found that a more complete and balanced assessment of the local air quality can be achieved only after taking into account the wind characteristics and emission factors of a much larger spatial scale than the initial (20 km by 20 km) study domain.

© 2018 Elsevier Ltd. All rights reserved.

1. Introduction

Due to social and economic reasons, coastal regions are often the preferred choices for urban and industrial developments. Air quality in a coastal region with industrial sources can be controlled not only by emissions but also by meteorology (Nester, 1995). For instance, many studies have explored the wind flows and boundary layer structures (Cheng et al., 2012; Liu et al., 2001; Melas et al., 1995; Ohara et al., 1989; Srinivas et al., 2007), topography (Cai and Steyn, 2000), sea surface temperature (Lee et al., 2011), urban

heat-island effect (Lin et al., 2008). Several studies also discussed the impact of land-sea breeze on air quality for coastal urban centers (Angevine et al., 2004; Cheng et al., 2012; Cheng, 2002; Clappier et al., 2000; Ding et al., 2004; Lalas et al., 1983; Lee et al., 2011; Lin et al., 2008; Liu and Chan, 2002; Liu et al., 2001; Ohara et al., 1989). The interplay between emissions and wind field could decide the overall air quality of a region. While episodes of strong land-sea interchanges were of obvious research interest, they by no means provided the sole perspective of the interplay between meteorology and air quality. The cause-and-effect relationship would be straightforward if the controlling wind field is monotonous to disperse a prominent emission source. However, the issue may not be trivial if the controlling wind field is complex, and the affecting parameters on air quality can extend far beyond the local domain. As a result, a systematic approach with the right tools of both observation and simulation with sufficient temporal

[☆] This paper has been recommended for acceptance by Dr. Hageman Kimberly Jill.

* Corresponding author.

** Corresponding author.

E-mail addresses: schen21@albany.edu (S.-P. Chen), cwang@cc.ncu.edu.tw (J.-L. Wang).

and spatial resolution, as well as geophysical scale, can be advantageous.

To test the approach of measurement–modeling coupling to study local air quality affected by major stationary sources, a rural coastal region with a gigantic petrochemical industrial complex (hereafter called the Complex) was chosen as the test ground. Refinery and associated processes within the Complex overwhelmed other possible sources in the region such as traffic due to the rural nature and scarce population. To give an idea of the prominence of the Complex and the contrast to other minor sources within the region, the Complex ranked among the world's top ten similar complexes in 2008, on a par with other major petrochemical companies in Germany, USA, Netherlands, UK, Saudi Arabia, and Japan (ArabianOilandGas.com). The Complex accommodated 70 associated plants, contributing approximately 10% to Taiwan's gross domestic product (GDP) in 2012 ([National Statistics, 2013](http://NationalStatistics.gov.tw)).

Due to the prominence of emissions, both air quality and wind parameters were intensively monitored surrounding the Complex to closely watch its emissions and to facilitate air-quality assessment in the area.

In this study, sulfur dioxide was selected as the target pollutant for both modeling and observations to track industrial emissions from and beyond this region due to the greater specificity of its source locations and amounts, as well as the sharp contrast between emissions and background than other pollutant species. The approach was to first validate the accuracy of the model simulations with the network observations, the simulations in turn provided the complete picture of the transport of industrial plumes. Therefore, the objective of this study is to use the tools of network observations and model simulations to approach the problem of how a major industrial source affects a rural area where the wind characteristics are highly seasonal. While most air-quality studies are urban-oriented with the widespread traffic as the major emission source to affect air quality, this study chooses a very different setting as a contrast; that is, an agricultural area with minimal traffic but a single major industrial source. Since the spatial coverage of the monitoring sites is believed to be unprecedented worldwide, the coupling of observations of high spatial-temporal resolution with the Eulerian model simulations presented here allows the air-quality assessment to be a benchmark for any region with major stationary emission sources.

2. Wind flow patterns at the coastal region

2.1. Monitoring sites (data source)

A network of more than 70 air quality stations are currently operated by Environmental Protection Administration of Taiwan (EPA-AQS) across the island reporting hourly concentrations (mixing ratios by volume) of NO_x, SO₂, CO, PM₁₀ and O₃. The AQS also report hourly wind data (wind speed and wind direction), temperature, humidity, rainfall, etc. In the study domain of interest, there are three EPA-AQS (E1–E3) situated at 3 km, 10 km, and 40 km towards inland from the coastline ([Fig. 1](#)).

In mid-2012, due to the prominence of the Complex, an additional network of nine continuous AQS were added within a radius of 20 km area (dubbed Petro-AQS) to closely watch the local air quality, forming a high-density network to synergistically characterize wind patterns and key pollutants with high temporal and spatial resolutions. One of the nine Petro-AQS was inside the Complex. The monitoring instruments at the nine Petro-AQS were maintained in accordance with the Taiwan EPA-AQS operation protocols ([Table S1](#)). As a result, data from the two different agencies can be directly inter-compared.

The following categorization of wind flow pattern is used to

systematically classify the daily wind field characteristics for the observations in this coastal area. The six-year worth of the EPA-AQS dataset from 2008 to 2013 were used to study the characteristic wind flow patterns over a broader coastal region ([Section 2.3](#)), whereas the observations from the more densely deployed Petro-AQS from Aug. 2013 to Jul. 2014 were utilized ([Section 2.4](#)) to gain more spatially resolved wind features in the vicinity of the Complex.

2.2. Categorization of surface wind patterns

In this coastal region of interest, the prevailing synoptic weather patterns are mostly determined by winter and summer monsoons ([Chang et al., 2000](#); [Chen et al., 2014](#); [Chiang et al., 2009](#)). The most dominant wind flows are northeasterlies mainly occurring in colder months. In summer, southwesterly winds are frequent; however, the land-sea breeze or more generally described as the local circulation (LC) can also be important. It was noted that high pollution events could occur during the land-sea breeze events in coastal areas ([Angevine et al., 2004](#); [Boucouvala and Bornstein, 2003](#); [Ding et al., 2004](#); [Kalthoff et al., 2005](#); [Klausner and Fattal, 2011](#); [Lin and Chang, 2002](#); [Talbot et al., 2007](#)).

To unravel the pollution phenomena in the study region of interest in a more systematic way which is largely wind driven, the three types of wind flows were categorized based on the perennial wind data obtained by the networks mentioned earlier ([Fig. 2](#)):

- (1) Northeast monsoonal (NEM)
- (2) Southwest monsoonal (SWM)
- (3) Local circulation (LC)

The monsoonal flow patterns are defined as the changes in wind direction confined within 90° within 24 h, which are manifested as higher wind speeds and rather monotonous wind directions over a fairly long period of days. Under this wind pattern, pollutants from afar can traverse long distances to affect downwind air quality.

For LC, including land-sea-breeze, the changes in wind direction are confined within 90°–270°. Under this flow pattern, pollutants from the coastal region tend to spread over a large area into inland.

Within each of the three wind flow types, most of the pollution episodes can be unambiguously described for the source origins and transport routes. Details of the analysis of area-wide wind flow patterns will be shown in [section 2.4](#).

2.3. Wind fields in a broader region

As seen in [Fig. 1](#), the three EPA-AQS (E1, E2 and E3) provided a lengthy meteorological dataset (2008–2013) not only in the coastal area, but also stretching far into the inland areas to the east (i.e., the E3 site). These hourly wind data revealed the overall wind characteristics for the entire region. In [Fig. 3](#) the statistics of the three wind flow patterns at these three EPA-AQS reveals that the percentages of the NEM pattern decreased from coast to inland. It ranged from 30% to 46% at the E1 site (coastal), but dropped to 22%–27% at E3 (inland). Likewise, the SWM pattern ranged from 7% to 12% at the E1 or E2 site, but reduced to 1%–4% at E3, suggesting that the monsoonal flows affect more in coastal areas than inland, but more so for NEM than for SWM. In contrast, for the LC flows, their percentages increased from 43% to 54% at E1 (coastal) to 69%–75% at E3 (inland), suggesting that the more inland areas are less affected by the monsoonal flows and more by the LC flows.

2.4. Wind fields within the target coastal region

When narrowing from the broader region down to the more

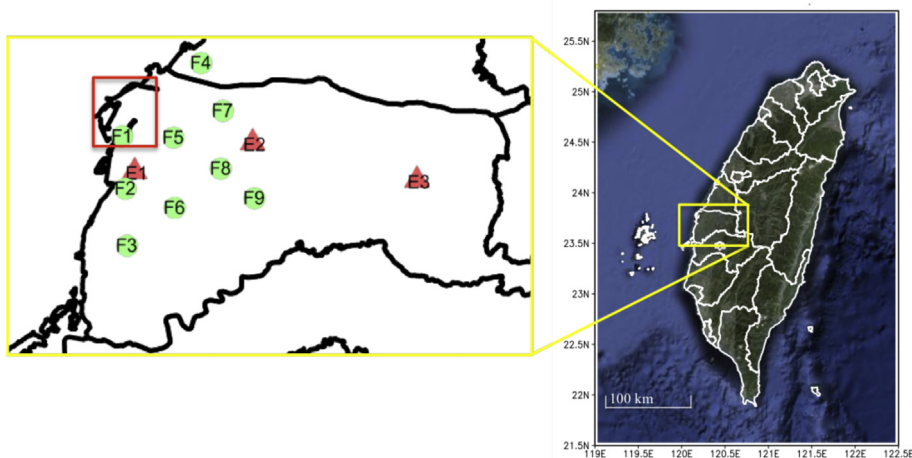
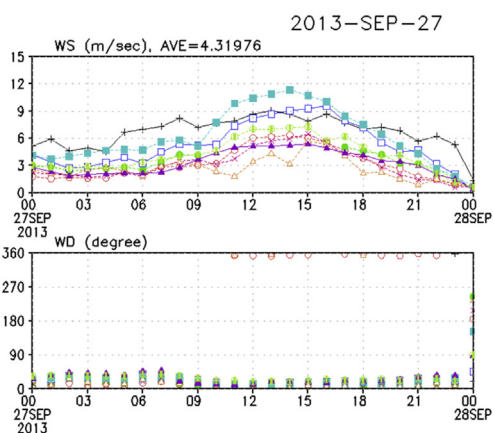
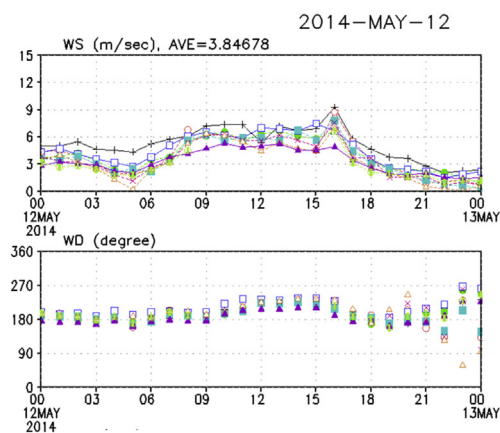


Fig. 1. The Petro- and EPA monitoring stations surrounding the coastal industrial complex. The nine Petro-AQS (green circles) were operated by the petrochemical complex as circled by the red box, while the three EPA-AQS (red triangles) were operated by Taiwan EPA. (For interpretation of the references to colour in this figure legend, the reader is referred to the Web version of this article.)

(A) NEM



(B) SWM



(C) LC

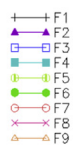
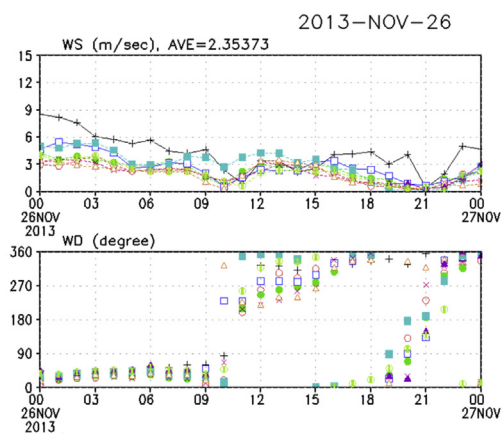


Fig. 2. Wind field observations at all Petro-AQS on three days corresponding to three different area-wide wind flow patterns. (A) Sep. 27, 2013 for the wind pattern of NEM, (B) May 12, 2014 for SWM and (C) Nov. 26 for LC.

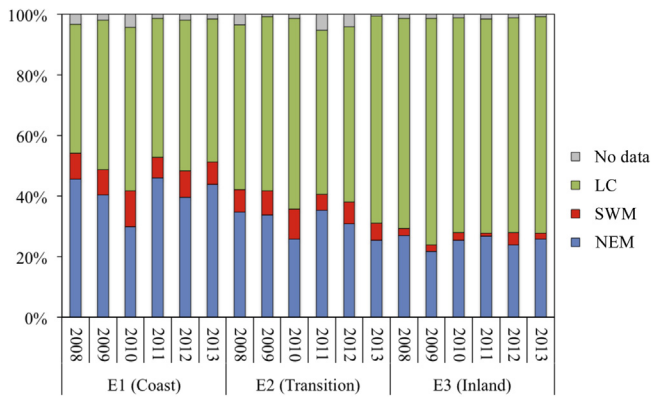


Fig. 3. Percentages of three surface wind patterns from the coast to inland based on the EPA-AQS data of three stations from 2008 to 2013 (refer to Fig. 1 for locations).

coastal area as defined by the eight Petro-AQS sites (from F2 to F9, excluding F1), the overall percentages of the three typical wind patterns were found to be rather consistent among all sites, and were also similar to the percentages for E1 or E3, indicating internal consistency for the data. The wind field observations at Petro-AQS surrounding the Complex were analyzed in the way that if the daily wind patterns at more than six of the eight sites were in agreement, then the area-wide wind pattern is determined as such. Fig. 4 and Table 1 displays the profiles and statistics of the monthly area-wide wind flow patterns from August 2013 to July 2014. Our statistics indicates that 82% of the days within a year (or at least more than 58% of the days within a month) had consistent area-wide wind flow patterns. Due to the varying dominant synoptic weather, the wind profiles showed pronounced seasonality (Fig. 4). As the weather system switched to the west Pacific sub-tropical high, the occurrence of the SWM flows pattern picked up in strength from 13% in May 2014 to 43% in June 2014. In summer months (e.g., July 2014 and August 2013), the LC was the dominant wind pattern with more than 50% of the day counts.

As a whole, the NEM and LC flows were the most occurred area-wide flow patterns in this coastal area, corresponding to 145 days (40%) and 130 days (36%) from 2013–Aug to 2014–Jul, respectively.

Because the determination of the area-wide flow patterns was somewhat arbitrary (i.e., at least six sites in the network showing the same wind flow pattern), this resulted in a number of days with

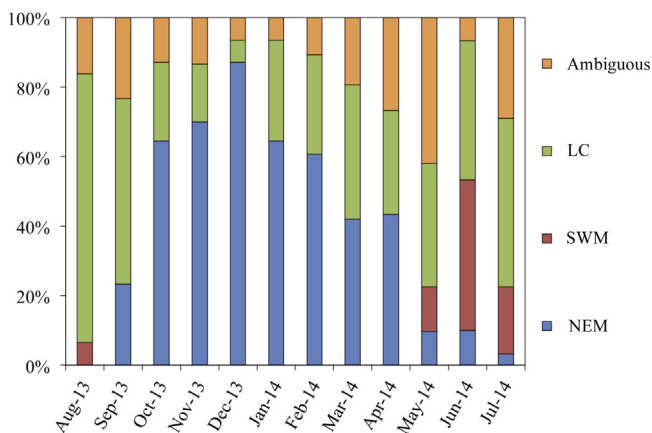


Fig. 4. Percentages of various area-wide wind patterns in the target coastal region based on Petro-AQS. The daily wind pattern was determined when more than six of the eight sites (F2–F9 outside coastal industrial complex) showed similar results. Ambiguous means winds cannot be clearly classified into the three typical patterns.

Table 1
Day counts for various wind flow patterns at coastal area^a.

Month	NEM	SWM	LC	Ambiguous	Sum
2013–Aug	0	2	24	5	31
2013–Sep	7	0	16	7	30
2013–Oct	20	0	7	4	31
2013–Nov	21	0	5	4	30
2013–Dec	27	0	2	2	31
2014–Jan	20	0	9	2	31
2014–Feb	17	0	8	3	28
2014–Mar	13	0	12	6	31
2014–Apr	13	0	9	8	30
2014–May	3	4	11	13	31
2014–Jun	3	13	12	2	30
2014–Jul	1	6	15	9	31
Sum	145	25	130	65	365

^a The daily wind pattern is defined when more than six of eight Petro-sites (excluding F1 site in coastal industrial park) showing similar daily wind flow patterns.

no clear classification into any specific wind type (18%), and thus are labeled as “ambiguous”. Since characterization of their influences on pollutant transport is complex, they are excluded from the current context.

3. Air pollutant transport under different wind flow patterns

In this study, SO₂ with its easily identified source locations is used as a tracer to illustrate the surface wind controlling the distributions of air pollutants from major sources affecting the target coastal region. Other pollutants, such as NO_x, CO, or volatile organic compounds, etc., have numerous sources by comparison, therefore their coupling with the wind patterns are not as clear.

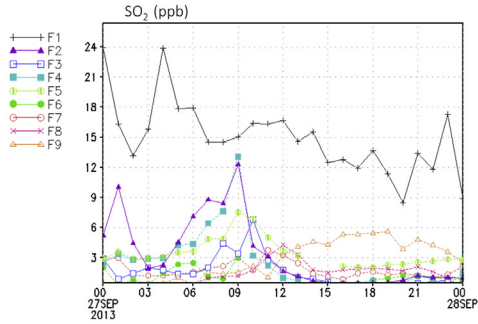
For the Petro-network, the distance between any two adjacent stations is less than 5 km (Fig. 1). Therefore, the high-density network is most likely to detect SO₂ plumes in the region. Through validation by the network measurements of both wind and SO₂, the model simulations can provide more realistic transport of pollutants. The Fifth-Generation Penn State/NCAR Mesoscale Model (MM5) and the three-dimensional Eulerian model (Chang et al., 2000) were used for meteorological and air quality simulations with nesting domain of 3 × 3 km² resolution from surface to 13.5 km above ground (see **Support Information** for details).

Fig. 5 shows the typical diurnal variations of SO₂ concentrations at all Petro-AQS for the three characteristic wind patterns of NEM, SWM and LC. The most influential sources of SO₂ can be identified for different wind patterns in the region, which are discussed as follows.

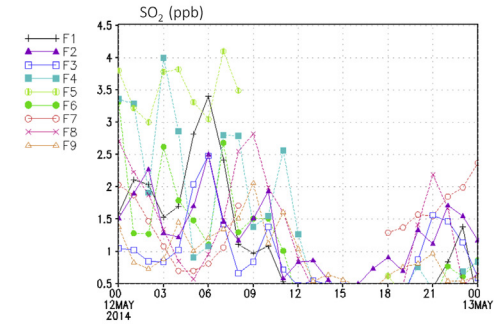
3.1. SO₂ distributions under monsoonal patterns

Fig. 5A shows an example of the surface wind field and SO₂ simulations for a typical NEM day (e.g., Sep. 27, 2013). During the NEM period the F1 site was right within the Complex and had the highest levels of SO₂ among all sites, often directly reflecting emissions from the nearby smokestacks within the Complex. On a typical day in the morning, the plume from the north coincided with that from the Complex under the strong northeasterlies to become one large plume to hit F2 and F4 (Fig. 5A–b1). While the F2 site directly reflected the emissions from the Complex, the F4 site, which is located upwind of the Complex, detected not the plumes from the Complex, but the ones from the northern source approximately 70 km north of the Complex. Consequently, the SO₂ mixing ratios at F1, F2 and F4 were the highest among all sites

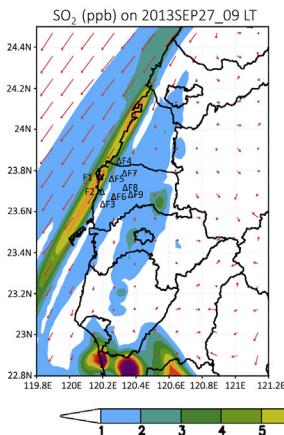
(A)-a 2013-09-27 (NEM)



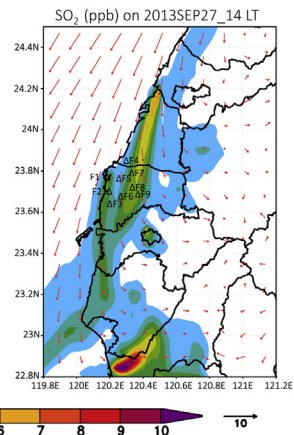
(B)-a 2014-05-12 (SWM)



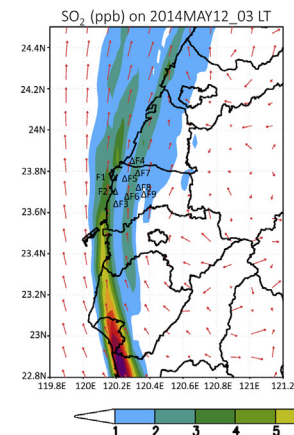
(A)-b1



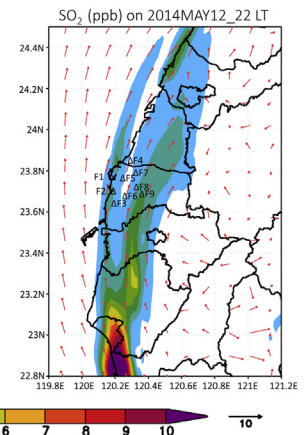
(A)-b2



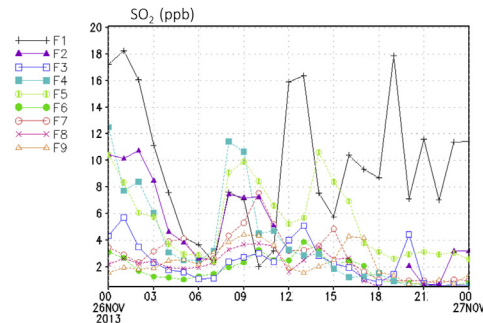
(B)-b1



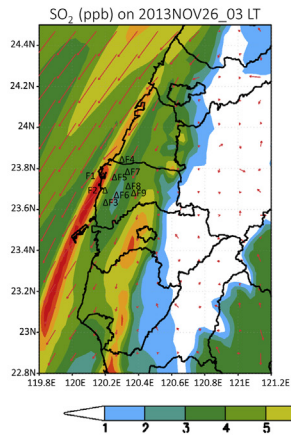
(B)-b2



(C)-a 2013-11-26 (LC)



(C)-b1



(C)-b2

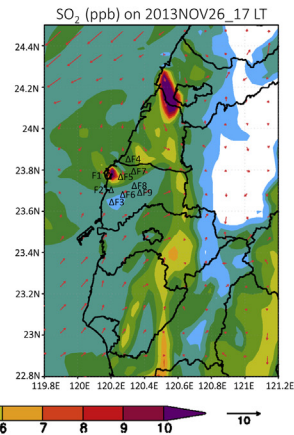


Fig. 5. Observations and simulations of SO₂ concentrations on three typical days corresponding to three different wind flow patterns of NEM (panel (A)-a, (A)-b1 and (A)-b2), SWM (panel (B)-a, (B)-b1 and (B)-b2) and LC (panel (C)-a, (C)-b1 and (C)-b2), respectively. Unit for surface wind is in m/sec.

during morning hours (Fig. 5A–a). The rest of the sites showed much less mixing ratios, because they were more on the east side and; hence, either only slightly encountered or largely missed the plumes (Fig. 5A–b1).

As the wind directions gradually swung from northeasterly to northerly as time elapsed into later hours, the two plume tracks began to decouple (Fig. 5A–b2) to cause site F2 (purple line in Fig. 5A–a) and F4 (light blue line in Fig. 5A–a) to decline rapidly in SO₂ mixing ratios. Noontime buoyancy lifted the plumes to pass over most sites, except F9 which was the farthest site to the south and may have touched the fringes of the diffused plumes to show slightly higher levels than most sites. Model simulations revealed that as the wind direction swung from NE to N as shown in Fig. 5A–b1, it became clear that another major source located 70 km north of the Complex also injected SO₂ into the target coastal region. Even though the Complex is the largest source of SO₂ in the target region, the contribution is dwarfed by the foreign northern source, which is the largest coal-burning fire power plant on the island with 5824 megawatt (MW) of output (Cheng, 2001) (area 2 in Fig. S4). As a result, the plumes of the power plant can sometimes be registered by the network. Therefore, in addition to the Complex as a major source of SO₂ affecting the target region, other northern sources may be even more important to affect the target coastal region under NEM.

Fig. 5B shows an example of the surface wind field and SO₂ simulations for a typical SWM day (e.g., May 12, 2014). Under the SWM pattern, the southern sources were transported to the target region by the southeasterly winds mostly occurred in summer. Most of the plumes from the south appeared to be confined to the coastal areas (Fig. 5B–b1 and -b2). Unlike the more confined air mixing under NEM, the long distance, higher mixing heights and more vigorous vertical mixing reduced the SO₂ levels at the surface (Fig. 5B–a), which when compared to the peak levels under NEM (Fig. 5A–a), were several times lower, falling within the range of 0.5–4 ppb at most sites, as shown in Fig. 5B–a. Even the F1 site within the Complex also showed much lower levels. The southerly plumes were lifted in the early afternoon due to strong convection to miss out most the Petro-sites as shown by the extremely low or non-detectable levels of SO₂ in the afternoon, and then touched down later to be detected by the network (Fig. 5B–a).

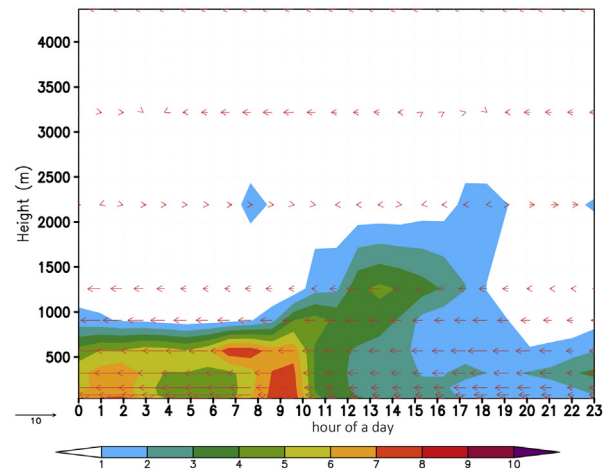
3.2. SO₂ distribution under LC pattern

In contrast to the more monotonous wind flows of both NEM and SWM, the LC flows tends to be more variable in the target coastal region. Fig. 5C shows an example of the surface wind field and SO₂ simulations for a typical LC day (e.g., Nov. 26, 2013). In this particular coastal region, the land-sea exchange is often coupled with LC. The land breeze often dominates before dawn, but the wind flows change into sea breeze after sunrise to become the dominant flows in daytime. The so-called LC can also be a transition between the monsoonal flows (by the synoptic system) and diffusion (by turbulence). The LC condition usually becomes more pronounced when the synoptic system weakens. As shown in Fig. 5C, the typical land-sea exchange occurred after 10 LT until the next day. But before 9 LT, the Siberian High dominated the coastal wind flows and remained northeasterly. Consequently, in early morning the SO₂ plume track from the two major sources of the fire power plant in the north and the Complex in the south coincided and appeared to be similar to Fig. 5A–b1. During this time period, the F1 site within the Complex and the F2 site south of the Complex picked up the petro-source directly. It was not until later in the morning to see the F4 site picking up the northern source of the power plant (Fig. 5C–b1). From then on, the synoptic system weakened and the LC tended to dominate the coastal region.

During this period, the atmosphere is very stagnant with very low wind speed, and the SO₂ plumes from both the Complex and the prominent northern source, i.e., the harbor industrial park, became very localized with minimal dispersion (Fig. 5C–b2). Under this circumstance, the much larger emission strength of the northern source became apparent.

The aforementioned different transport behaviors of a pollutant under different flow patterns can be further viewed from the vertical point of view. Fig. 6 displays the cross-section of the wind fields and SO₂ distributions at site F1 (within the Complex) by comparing the two distinct wind patterns of NEM and LC. Under NEM (Fig. 6A), one can see that most of the zonal surface wind flows were from the east (from land to sea) throughout the day in the coastal region. The wind direction was very consistent above the ground to 1.3 km, manifesting the work zone of the synoptic weather flows near the surface. In contrast, under LC (Fig. 6B), the land breeze was apparent before dawn, but the weaker sea breeze in daytime tended to accumulate SO₂ within the near-surface atmosphere, as has also depicted in Fig. 5C–b2. As a result, combining Fig. 5C with Fig. 6 provides a more complete understanding of both horizontal and vertical distributions to illustrate that emissions of a pollutant affecting the target area is not only sensitive to the

(A) 2013-09-27 (NEM)



(B) 2013-11-26 (LC)

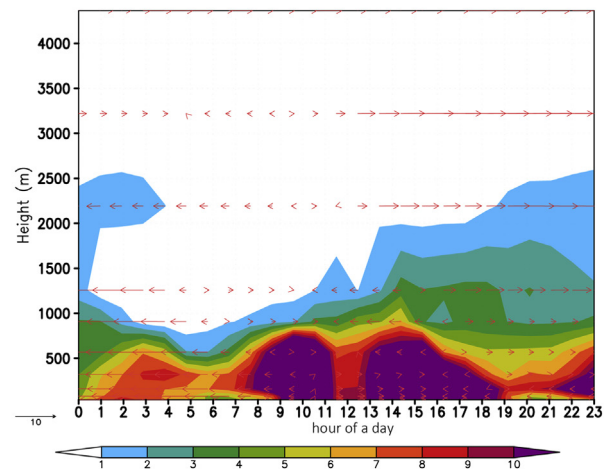


Fig. 6. Cross-section of vertical wind field (m/sec) and surface SO₂ (ppb) simulations at the coastal Petro-complex on two typical days of (A) Sep. 27, 2013 for the NEM wind pattern and (B) Nov. 26, 2013 for the LC wind pattern.

locations or sheer size of the sources but even more to the atmospheric conditions for transport.

4. Conclusions

The coupling of network measurements with model simulations is an effective approach to assess the impact of prominent industrial emissions on air quality. To facilitate demonstration of the approach, SO₂ was employed as a tracer of industrial emissions with high-resolution measurements and model simulations. The wind field classified into three types of highly seasonal dependence allowed a more systematic approach to attribute the received pollution not only to the Complex, but also the sources from afar. It was concluded that even though a seemingly prominent local source could easily be perceived as the single most important polluter to affect local air quality, multiple prominent sources from afar also played a significant role to affect the local air quality. As a result, a more complete and balanced assessment of the local air quality can only be achieved when taking into account the meteorological and emission factors of a much broader scale than the study domain of interest. The lack of any one of the two tools, either the network observations or modeling, would seriously hamper the interpretation of the received pollutants.

Acknowledgments

We thank the Taiwan Environmental Protection Administration and Formosa Plastics Group for providing the air quality and meteorological monitoring data.

Appendix A. Supplementary data

Supplementary data related to this article can be found at <https://doi.org/10.1016/j.envpol.2018.01.091>.

References

- Angevine, W.M., Senff, C.J., White, A.B., Williams, E.J., Koermer, J., Miller, S.T.K., Talbot, R., Johnston, P.E., McKeen, S.A., Downs, T., 2004. Coastal boundary layer influence on pollutant transport in New England. *J. Appl. Meteorol.* 43, 1425–1437.
- Boucouvala, D., Bornstein, R., 2003. Analysis of transport patterns during an SCOS97-NARSTO episode. *Atmos. Environ.* 37 (Suppl. 2), 73–94.
- Cai, X.M., Steyn, D.G., 2000. Modelling study of sea breezes in a complex coastal environment. *Atmos. Environ.* 34, 2873–2885.
- Chang, K.-H., Jeng, F.-T., Tsai, Y.-L., Lin, P.-L., 2000. Modeling of long-range transport on Taiwan's acid deposition under different weather conditions. *Atmos. Environ.* 34, 3281–3295.
- Chen, S.-P., Liu, W.-T., Ou-Yang, C.-F., Chang, J.S., Wang, J.-L., 2014. Optimizing the emission inventory of volatile organic compounds (VOCs) based on network observations. *Atmos. Environ.* 84, 1–8.
- Cheng, F.-Y., Chin, S.-C., Liu, T.-H., 2012. The role of boundary layer schemes in meteorological and air quality simulations of the Taiwan area. *Atmos. Environ.* 54, 714–727.
- Cheng, W.-L., 2001. Synoptic weather patterns and their relationship to high ozone concentrations in the Taichung Basin. *Atmos. Environ.* 35, 4971–4994.
- Cheng, W.-L., 2002. Ozone distribution in coastal central Taiwan under sea-breeze conditions. *Atmos. Environ.* 36, 3445–3459.
- Chiang, C.-K., Fan, J.-F., Li, J., Chang, J.S., 2009. Impact of Asian continental outflow on the springtime ozone mixing ratio in northern Taiwan. *J. Geophys. Res.: Atmos.* 114, D24304.
- Clappier, A., Martilli, A., Grossi, P., Thunis, P., Pasi, F., Krueger, B.C., Calpini, B., Graziani, G., van den Bergh, H., 2000. Effect of sea breeze on air pollution in the greater Athens area. Part I: numerical simulations and field observations. *J. Appl. Meteorol.* 39, 546–562.
- Ding, A., Wang, T., Zhao, M., Wang, T., Li, Z., 2004. Simulation of sea-land breezes and a discussion of their implications on the transport of air pollution during a multi-day ozone episode in the Pearl River Delta of China. *Atmos. Environ.* 38, 6737–6750.
- Kalthoff, N., Kottmeier, C., Thürauf, J., Corsmeier, U., Säid, F., Fréjafon, E., Perros, P.E., 2005. Mesoscale circulation systems and ozone concentrations during ESCOMPTE: a case study from IOP 2b. *Atmos. Res.* 74, 355–380.
- Klausner, Z., Fattal, E., 2011. An objective and automatic method for identification of pattern changes in wind direction time series. *Int. J. Climatol.* 31, 783–790.
- Lalas, D.P., Asimakopoulou, D.N., Deligiorgi, D.G., Helmis, C.G., 1983. Sea-breeze circulation and photochemical pollution in Athens, Greece. *Atmos. Environ.* 1967 (17), 1621–1632.
- Lee, S.-H., Lee, H.-W., Kim, Y.-K., Jeon, W.-B., Choi, H.-J., Kim, D.-H., 2011. Impact of continuously varied SST on land-sea breezes and ozone concentration over south-western coast of Korea. *Atmos. Environ.* 45, 6439–6450.
- Lin, C.-H., Chang, L.-F.W., 2002. Relative source contribution analysis using an air trajectory statistical approach. *J. Geophys. Res.: Atmos.* 107, 4583.
- Lin, C.-Y., Chen, F., Huang, J.C., Chen, W.C., Liou, Y.A., Chen, W.N., Liu, S.-C., 2008. Urban heat island effect and its impact on boundary layer development and land-sea circulation over northern Taiwan. *Atmos. Environ.* 42, 5635–5649.
- Liu, H., Chan, J.C.L., 2002. An investigation of air-pollutant patterns under sea-land breezes during a severe air-pollution episode in Hong Kong. *Atmos. Environ.* 36, 591–601.
- Liu, H., Chan, J.C.L., Cheng, A.Y.S., 2001. Internal boundary layer structure under sea-breeze conditions in Hong Kong. *Atmos. Environ.* 35, 683–692.
- Melas, D., Ziomas, I.C., Zerefos, C.S., 1995. Boundary layer dynamics in an urban coastal environment under sea breeze conditions. *Atmos. Environ.* 29, 3605–3617.
- National Statistics, R.T., 2013. National Accounts.
- Nester, K., 1995. Influence of sea breeze flows on air pollution over the Attica peninsula. *Atmos. Environ.* 29, 3655–3670.
- Ohara, T., Uno, I., Wakamatsu, S., 1989. Observed structure of a land breeze head in the Tokyo metropolitan area. *J. Appl. Meteorol.* 28, 693–704.
- Srinivas, C.V., Venkatesan, R., Bagavath Singh, A., 2007. Sensitivity of mesoscale simulations of land-sea breeze to boundary layer turbulence parameterization. *Atmos. Environ.* 41, 2534–2548.
- Talbot, C., Augustin, P., Leroy, C., Willart, V., Delbarre, H., Khomenko, G., 2007. Impact of a sea breeze on the boundary-layer dynamics and the atmospheric stratification in a coastal area of the North Sea. *Boundary-Layer Meteorol.* 125, 133–154.